The Astrophysical Journal, 995:66 (11pp), 2025 December 10 https://doi.org/10.3847/1538-4357/ae1138

Fermi-LAT Captures a Late-2024 Gamma-Ray Outburst near Two Newly Identified Gamma-Ray-emitting Galactic Supernova Remnants, without Evidence of Physical Association

Miltiadis Michailidis[1,2,3], Marianne Lemoine-Goumard[4], Niccolo Di Lalla[1,2,3], Nicola Omodei[1,2,3], C. C. Cheung[5], Guillem Marti-Devesa[6,7], and Denis Bernard[8]
[1] W. W. Hansen Experimental Physics Laboratory (HEPL), USA; milmicha@stanford.edu
[2] Kavli Institute for Particle Astrophysics and Cosmology (KIPAC), USA
[3] Department of Physics and SLAC National Accelerator Laboratory, Stanford University, Stanford, CA 94305, USA
[4] Univ. Bordeaux, CNRS, LP2i Bordeaux, UMR 5797, F-33170 Gradignan, France
[5] Naval Research Laboratory, Space Science Division, DC 20375, USA
[6] Dipartimento di Fisica, Universitá di Trieste, I-34127 Trieste, Italy
[7] Istituto Nazionale di Fisica Nucleare, Sezione di Trieste, 34127 Trieste, Italy
[8] LLR, Ecole polytechnique, CNRS/IN2P3 and IPP, 91128 Palaiseau, France
Received 2025 September 1; revised 2025 September 28; accepted 2025 October 7; published 2025 December 4

Abstract

We report the gamma-ray study of two neighboring in the sky Galactic supernova remnants (SNRs), namely, 3C 434.1 (or G094.0+01.0) and G093.7–00.2. In the vicinity of the two SNRs, a late-2024 gamma-ray outburst—not physically connected to the SNRs—was detected with the Fermi Large Area Telescope (LAT). Employing 16.5 yr of Fermi-LAT data, we report the first firm detection of the gamma-ray counterpart of 3C 434.1 at a 7.2σ significance and a likely detection of an enhanced gamma-ray emission signal at a 4.5σ level from G093.7–00.2. The late-2024 gamma-ray outburst is detected at a $\sim 12\sigma$ significance level over a duration of 3 days. For all three objects, a comprehensive morphological and spectral analysis of the corresponding gamma-ray data was conducted. The prevalent scenario for the nature of the gamma-ray emission of both SNRs is attributed to their surrounding environment. Both are likely interacting with nearby dense material, resulting in hadronically induced gamma-ray emission. We deduce that the outburst source is most likely a blazar in flare, linked to the compact, flat-spectrum radio source TXS 2138+527 (also known as NVSS J213953+530016). Further, the spectral analysis of the gamma-ray source conducted within the 100 MeV–800 GeV energy range using the complete LAT data sets, which yielded a soft averaged spectral shape, supports the hypothesis of a flat spectrum radio quasar (FSRQ) origin for the source; with a most likely leptonically induced scenario for the observed gamma-ray outburst as inferred from the obtained hard spectral shape when utilizing short time intervals focusing on the outburst.

Unified Astronomy Thesaurus concepts: Supernova remnants (1667); Blazars (164); High energy astrophysics (739); Gamma-ray sources (633)

1. Introduction

Astrophysical objects, both Galactic and extragalactic, demonstrate a range of particle acceleration mechanisms, resulting in diverse gamma-ray emission profiles. These profiles may manifest as transient sources of highly energetic, short-duration gamma-ray emissions, such as those observed in gamma-ray bursts (GRBs), active galactic nuclei (AGN), tidal disruption events (TDEs), supernovae (SNe), and novae. Alternatively, they may appear as persistent, longer-duration emitters with lower energy outputs, exemplified by supernova remnants (SNRs), pulsar wind nebulae (PWNe), and pulsars (PSR). In this study, we examine gamma-ray emission that may originate from one or more of these source classes. We focus on the relevant subtypes of AGN and SNRs.

SNRs. SNRs are frequently characterized as the noncompact endpoints of supernova explosions or as stellar graveyards, typically manifesting as shell-like structures in the sky. These structures can be heavily distorted depending on their surrounding ambient medium and are bounded by an expanded shock. They represent the debris of stellar ejected material and the swept-up interstellar medium and are observable across the entire electromagnetic (EM) spectrum, exhibiting both thermal and/or nonthermal signatures contingent upon the wavelength observed. The fraction of Galactic SNRs, currently numbering around 300 confirmed cases (D. A. Green 2025a, 2025b), primarily identified through radio surveys, that are bright in gamma-rays is relatively small. There are only 30–40 cases of detected gamma-ray sources with compelling evidence for association with known SNRs from multifrequency studies (e.g., A. Giuliani & M. Cardillo 2024 and references therein). Although not all Galactic SNRs are expected to be detected in gamma-rays—since SNRs emit at different wavelengths depending on their evolutionary stage and because their particle acceleration efficiency varies with intrinsic properties and progenitor origin—increasing the number of detected gamma-ray SNRs remains crucial. In particular, identifying those with evidence of hadronically induced gamma-ray emission is essential for unraveling the proportion of different source contributions in the cosmic ray (CR) spectrum. SNRs that show apparent interaction with nearby dense atomic and

molecular material are among the strongest candidates to exhibit hadronic gamma rays.

In this context, both 3C 434.1 (or G094.0+01.0) and G093.7–00.2 (or CTB 104A or DA 551) are Galactic SNRs that appear close by in the sky and are considered to be interacting with dense material and thus represent prominent targets for searching for extended gamma-ray emission. Since their initial radio detection (K. S. Yang & J. R. Dickel 1965; J. L. Caswell 1970; A. G. Willis 1973), radio observations across various frequencies utilizing different radio telescopes, such as Effelsberg, the Dominion Radio Astrophysical Observatory (DRAO), and the Urumqi 25 m telescope (F. Mantovani et al. 1982; T. L. Landecker et al. 1985; X. Y. Gao et al. 2011; X. H. Sun et al. 2011), have contextualized new observations with older flux measurements. This has resulted in nonthermal radio indices of −0.45 and −0.52 (for $S_\nu \propto \nu^\alpha$, K. Rohlfs 1990) for 3C 434.1 and G093.7–00.2, respectively, thereby classifying the extended radio emission as SNRs. More recently, T. Foster (2005) and B. Uyaniker et al. (2002) have provided high-resolution radio continuum maps of these two remnants using data from the Canadian Galactic Plane Survey (CGPS). Currently, a radio angular extension of $30' \times 25'$ for 3C 434.1 and $80'$ for G093.7–00.2 is reported by synthesizing all available radio data for the two SNRs.

To date, G093.7–00.2 has been solely detected in radio continuum. In contrast, 3C 434.1, an SNR that has been studied more extensively, has shown indications of enhanced optical emission, as observed with Alberta's Devon Astronomical Observatory (DevonAO)(T. Foster 2005), and confirmed thermal extended X-ray emission observed with ROSAT (T. Foster 2005), except for a small southern region of the remnant that exhibits hard X-ray emission likely of nonthermal origin, as observed with XMM-Newton (V. Doroshenko et al. 2019). These studies indicate that the remnant exhibits spatially coincident enhanced emission in all three wavelengths toward its eastern half, with a distance estimate of 4.5 kpc. This distance estimate, based on the model developed by T. Foster & D. Routledge (2003), is higher than the 3.0 kpc kinematic distance derived from the systemic velocity of the molecular cloud likely associated with the remnant, as reported by I.-G. Jeong et al. (2013). Recent optical extinction studies support the closer distance to Earth for 3C 434.1 reported by I.-G. Jeong et al. (2013), estimating the remnant's distance at 2.5 ± 1.1 kpc (H. Zhao et al. 2020). Further, I.-G. Jeong et al. (2013) provide a young age estimate of 8 kyr based on the Sedov self-similar solution, while T. Foster (2005) reports a rather middle-aged ∼25 kyr remnant based on an alternative explanation incorporating the theory of supernovae interaction with circumstellar bubbles (R. A. Chevalier & E. P. Liang 1989) and constrained by radio and X-ray observations. A progenitor origin likely exceeding a mass of $8M_\odot$, indicating a core-collapse remnant origin expanding in the wind bubble cavity of its massive progenitor, is reported in T. Foster (2005). However, no associated compact remnant objects have been identified to date. In comparison to 3C 434.1, G093.7–00.2 is reported to be located at a closer distance, with B. Uyaniker et al. (2002) placing the SNR at 1.5 ± 0.2 kpc based on the kinematics of the H I structure, while recent optical extinction studies report marginally larger distance estimates of 2.16 ± 0.02 kpc and 1.99 ± 0.33 (S. Wang et al. 2020; H. Zhao et al. 2020). For G093.7–00.2, there are no firm age estimates. Nonetheless, B. Uyaniker et al. (2002) report an old SNR (well above a few tens of kyr), as deduced from the global spectral index and its magnetic field configuration, and F. Yamamoto et al. (2002) provide an age estimate ranging from 29 to 74 kyr.

Regarding gamma-ray signatures, V. Doroshenko et al. (2019) utilized nearly 10 yr of Fermi Large Area Telescope (LAT) data in the 0.1–300 GeV range, presenting evidence for a gamma-ray emission component with a significance of approximately 4σ, potentially linked to 3C 434.1. However, they did not adequately account for the degrees of freedom (dof) introduced by the inclusion of an additional point source in their model, which involved 4 dof, that is, two spatial and two spectral parameters allowed to vary, in their calculation of gamma-ray signal significance. When this factor is considered, the significance for 3C 434.1 would be adjusted to 3.2σ. Further, V. Doroshenko et al. (2019) suggested a connection between the hard nonthermal X-ray filament found at the southern part of the remnant and the enhanced gamma rays. Notably, the remnant's unusual radio morphology can be explained by an interaction with a thin CO cloud located on its western hemisphere, supported by the results of hydrodynamical evolutionary modeling reported in I.-G. Jeong et al. (2013). In contrast, for G093.7–00.2, V. Doroshenko et al. (2019) reported a weaker gamma-ray signal with a significance of $\sim 3\sigma$. Accounting for dof, the appropriate significance value should be 1.7σ. Additionally, signatures of the remnant's interaction with surrounding neutral material have been identified (B. Uyaniker et al. 2002). These associations will be further examined in this work based on 16.5 yr of Fermi-LAT gamma-ray data. Notably, no gamma-ray detection has been reported for either remnant in the first Fermi-LAT SNR catalog (F. Acero et al. 2016).

Transients. Transients are extreme, short-lived events characterized by significant variability, either due to the partial or total destruction of an astrophysical object or through accretion mechanisms where compact objects accrete material from a companion donor or infalling matter, leading to the release of gamma-ray emission (among other components) through nuclear processes or eruptions in the form of narrow beams of relativistic charged particles.

This study focuses on a specific category of transient events: blazars. In the prevailing unification model of AGN, a blazar is conceptualized as a radio-loud AGN with a relativistic jet oriented toward the observer (R. D. Blandford & M. J. Rees 1978). This orientation introduces an enhancement of the observed emission due to Doppler boosting effects, making blazars gamma-ray loud AGNs. The bright gamma-ray emission is believed to originate when observing directly through the narrow jet of these objects. The infall of matter onto the central supermassive black hole of these galaxies powers their peculiar behavior and energetic features (e.g., jets). Depending on the strength of their optical emission lines, blazars can be further classified as BL Lacertae–type objects (BL Lac objects) or flat-spectrum radio quasars (FSRQs; see C. M. Urry & P. Padovani 1995). The former exhibit weak optical lines, whereas the latter are characterized by strong and broad optical emission lines. For a more comprehensive discussion of the general properties of BL Lac objects and FSRQs, refer to A. A. Abdo et al. (2010a) and references therein.

The challenge with these transient classes is that these events occur randomly across the entire sky, and although they can be readily detected by Fermi-LAT (S. Chaty 2012;

L. Baldini et al. 2021), confident classification is difficult due to limited localization accuracy, especially for transients positioned in complex and crowded regions typically close to the Galactic plane, at $|b| < 10°$. To this end, multi-wavelength observations are crucial for gaining further insight into the nature and origin of these events.

In this study, we explore potential gamma-ray signals from the two nearby SNRs likely interacting with dense material, and investigate a gamma-ray outburst event that took place on August 7, 2024, in their near vicinity, utilizing 16.5 yr of Fermi-LAT data. Section 2 details the Fermi-LAT data employed for this study, as well as the data reduction processes. In Section 3, we outline the detailed morphological analysis employed to model the detected gamma-ray emission from the two remnants and the outburst event. Section 4 presents the gamma-ray spectral analysis results for all three sources. Section 5 provides a time-resolved analysis of the gamma-ray outburst and a discussion of the possible origins indicated by multiwavelength information. Section 6 offers discussion, scientific interpretation, and concluding remarks.

2. LAT Data Reduction

We utilize the complete 16.5 yr data set from the Fermi-LAT Pass 8 (P8R3) data (P. Bruel et al. 2018), spanning from the mission's start of scientific data acquisition on August 8, 2008, to February 13, 2025. This period corresponds to mission elapsed time (MET) from 239557417 to 761167438. Our analysis focuses on a $20° \times 20°$ region centered on the G093.7–00.2 SNR (R.A.: $322\overset{\circ}{.}32$, decl.: $50\overset{\circ}{.}83$). The 3C 434.1 SNR and the outburst event are located $\sim 1\overset{\circ}{.}3$ and $\sim 2\overset{\circ}{.}7$ from the region of interest (ROI) center, respectively. We adapted standard LAT data reduction procedures and divided the time selections into shorter time intervals to analyze the outburst. To minimize Earth limb contamination while optimizing data statistics, we set maximum zenith angle thresholds of 90° and 105° for LAT data analysis at photon energies >100 MeV and >1 GeV, respectively. The SOURCE event class, with all event types included (evtype = 3), was employed alongside the latest instrument response functions (IRFs), `P8R3_SOURCE_V3`. Analysis tasks were conducted using the `fermipy` analysis software v.1.3.1 (M. Wood et al. 2017), which provides a sophisticated Python interface for executing *fermitools* v.2.2.0[9] tasks within a binned likelihood analysis framework. Our initial model incorporates all Fermi-LAT Fourth Source Catalog Data Release 4 (4FGL-DR4) sources (S. Abdollahi et al. 2022; J. Ballet et al. 2023) within a $30° \times 30°$ region from our analysis center, along with two distinct background components: `gll_iem_v07.fits` and `iso_P8R3_SOURCE_V3_v1.txt`, which account for the Galactic diffuse and isotropic background contributions, respectively. Among the three sources examined, only 3C 434.1 is spatially coincident with a 4FGL-DR4 source (see upper left panel of Figure 1). The latter 4FGL-DR4 source, namely, 4FGL J2123.9+5158, is excluded from the model to investigate the gamma-ray emission from 3C 434.1. In all fitting steps, we let the spectral parameters of all sources within 3° of the analysis center, the normalization of the two background components, and the index of the Galactic diffuse component vary. A pixel size of $0\overset{\circ}{.}02$ was employed to ensure adequate imaging resolution given the small angular size of the objects of interest ($30' \times 25'$ for 3C 434.1 and $80'$ for G093.7–00.2 as described in Section 1), along with eight logarithmic energy bins per decade. We conducted a morphological analysis of the two SNRs and the outburst event using the complete 16.5 yr of available LAT data at energies >1 GeV, a range that provides an improved LAT point-spread function (PSF) for detailed spatial analysis. However, given the gamma-ray contribution from both SNRs in the 500 MeV–1 GeV range, we utilize the 500 MeV–800 GeV energy range to report a test statistic (TS) value of TS = 66.1 (7.2σ) and TS = 29.3 (4.5σ) detection of the two SNRs, employing the best-fit spatial templates outlined in Section 3 for each. Throughout this study, the TS value is consistently defined as $\mathrm{TS} = 2(\ln\mathcal{L}_1 - \ln\mathcal{L}_0)$, representing the logarithm of the ratio of the tested hypothesis likelihood ($\mathcal{L}_1$) and the null hypothesis likelihood ($\mathcal{L}_0$). The spectral analysis was performed over the broader energy range of 100 MeV–800 GeV for all three sources, again utilizing the full LAT data sets. Regarding the outburst event primarily detected at energies > 1 GeV, the time-resolved analysis is performed in single-day bins and 6 hr time bins over a 5 day period centered on the peak day of the event, August 7, 2024. Additional spectral analysis was performed in short time intervals of 6 hr, 18 hr, and 3 days during the outburst period.

[9] https://fermi.gsfc.nasa.gov/ssc/data/analysis/software/

3. Morphological Analysis

3.1. 3C 434.1

Although 3C 434.1 was initially reported as a nondetected SNR in the first SNR Fermi catalog (F. Acero et al. 2016), the most recent 4FGL-DR4 catalog includes a point source, designated 4FGL J2123.9+5158, which is spatially coincident with the SNR. Consequently, this source was excluded from our model (constructed as described in Section 2) to characterize the gamma-ray emission coincident with the SNR (see Figure 1, upper left panel). We assess any evidence of extension using geometrical templates, that is, the radial disk and radial Gaussian spatial templates, as well as a custom spatial template generated from the CGPS radio observation of the SNR after setting all pixel values to zero outside the remnant's extension. In all cases, there is substantial improvement of the fit relative to the point source (4FGL J2123.9+5158; see Table 1). The quality of the fit is evaluated using the Akaike information criterion (AIC; H. Akaike 1974), which evaluates the goodness of fit between the different models by $\Delta\mathrm{AIC} = \mathrm{AIC}_{\mathrm{point\ source}} - \mathrm{AIC}_i = 2(\Delta\mathrm{dof} - \mathcal{L})$, where i corresponds to the radial disk, radial Gaussian, and radio templates, and $\mathcal{L}$ represents the likelihood estimate. As indicated in Table 1, a radial disk (model 4) provides the best description of the gamma-ray emission from the SNR location according to the AIC criterion, yielding a $\mathrm{TS}_{\mathrm{ext}} = 23.4$. Thus, we conclude that the gamma-ray emission is significantly extended, likely representing the gamma-ray counterpart of the 3C 434.1 SNR in the absence of other identified objects in this region. A TS = 61.35, which for the 5 dof introduced by the radial disk spatial template, results in a 6.9σ detection significance >1 GeV. Subsequently, we generate a zoomed-in PS (for ``p-value statistic'') map centered on the remnant's coordinates (left panel of Figure 2) and explore correlation features between the radio emission from 3C 434.1 and its likely associated molecular cloud, discovered in I.-G. Jeong et al. (2013), with the detected extended gamma-ray emission.

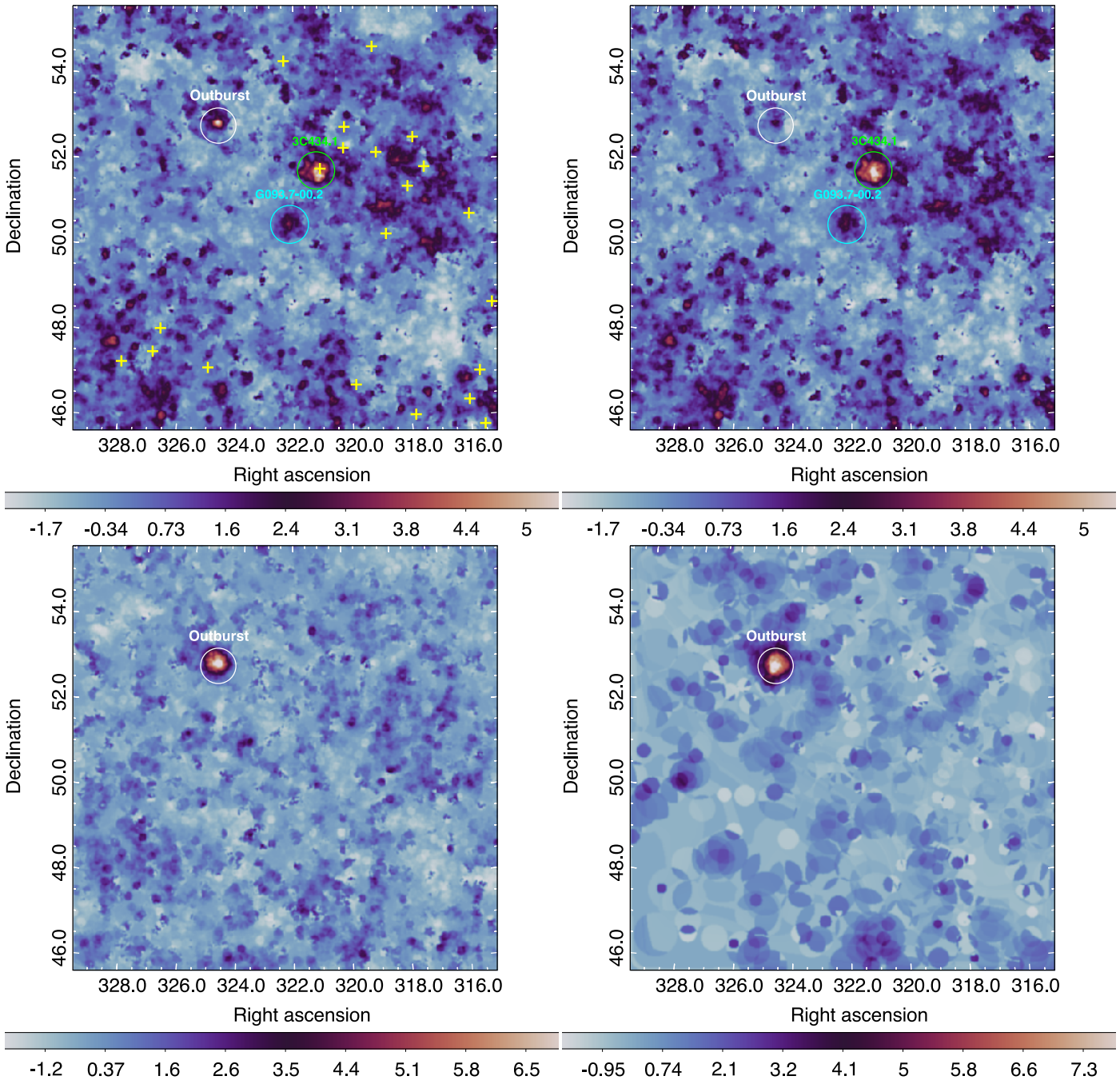

Figure 1. The 10° × 10° Fermi-LAT PS maps, expressed in sigmas (σ) and for energies >1 GeV, are centered at G093.7–00.2. PS maps are deviation probability maps that offer an accurate data and model comparison by being sensitive to both positive and negative deviations (P. Bruel 2021). Coordinates are given in degrees. The model excludes only the spatially coincident 4FGL J2123.9+5158 source with the 3C 434.1 SNR. Circles indicate the positions of the two SNRs and the outburst event (located ∼0.°26 above the Galactic plane). Yellow crosses indicate 4FGL-DR4 sources within the ROI. The upper left panel presents the Fermi map for the entire 16.5 yr time range. The upper right panel displays the Fermi map with the first 14 yr of data from August 8, 2008, to August 8, 2022 (MET: 239557417 to 681320621). The lower left panel shows the Fermi map with the last 2.5 yr of data from August 8 2022, to February 13, 2025 (MET: 681320621 to 761167438). The lower right panel illustrates the Fermi map with 5 days of data from August 5, 2024, to August 10, 2024 (MET: 744552005 to 744984005) centered on the event peak.

Interestingly, while the radio and X-ray emission are particularly enhanced toward the eastern hemisphere of the SNR (T. Foster 2005; V. Doroshenko et al. 2019), this is not where the detected gamma-ray emission peaks (left panel of Figure 2). Instead, we observe enhanced gamma-ray emission in the western hemisphere of the SNR, which is also where the SNR spatially overlaps with dense molecular material, as shown in I.-G. Jeong et al. (2013). Therefore, we propose that the nature of the gamma-ray emission arises from proton–proton interactions facilitated by the presence of dense material in the region where the SNR expands.

3.2. G093.7–00.2

There are no 4FGL-DR4 sources identified within the region where the G093.7–00.2 SNR extends. Given the availability of

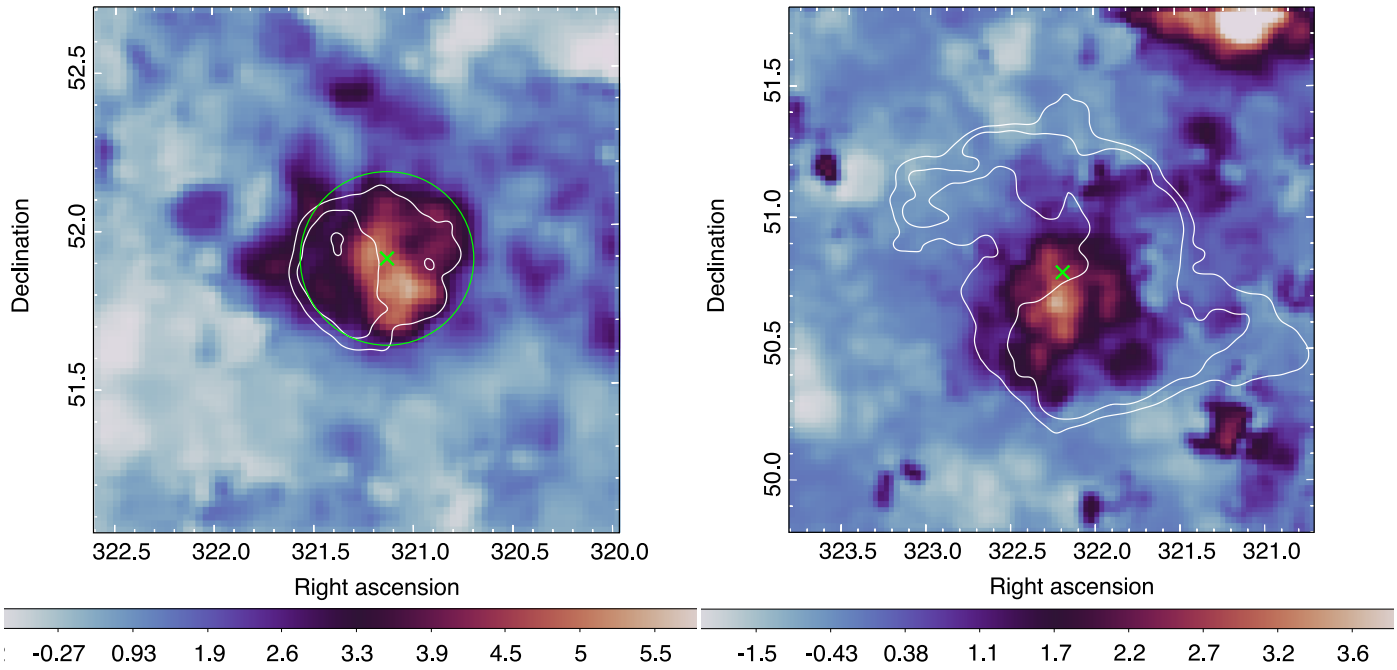

Figure 2. The Fermi-LAT PS maps, expressed in sigmas (σ) and for energies >1 GeV, are centered on the SNRs 3C 434.1 (left panel) and G093.7–00.2 (right panel). Coordinates are given in degrees. The white contours delineate the CGPS radio extensions of the SNRs in their respective panels. The best-fit location and extension of the gamma-ray sources are displayed in green. There is no measured extension for G093.7–00.2. The prominent feature in the upper right corner of the right panel map corresponds to the gamma-ray counterpart of 3C 434.1.

Table 1
Comparison of the Goodness of Fit of Different Spatial Templates Tested for the Two SNRs and the Outburst, >1 GeV

Model Number	Spatial Template	TS	LogLikelihood	dof	ΔAIC	R.A., decl. (J2000, deg)	R° or σ	TS_{ext}
	No 4FGL J2123.9+5158		−1011547.58					
			3C 434.1					
1	4FGL J2123.9+5158	55.37	−1011520.49	4	null	⋯	⋯	⋯
2	Radio CGPS	54.69	−1011520.77	2	3.44	⋯	⋯	⋯
3	2D-Gauss	59.42	−1011518.81	5	1.36	321.09 ± 0.05, 51.91 ± 0.05	$0.17^{+0.05}_{-0.04}$	22.6
4	2D-Disk	61.35	−1011517.72	5	3.54	321.11 ± 0.04, 51.91 ± 0.04	$0.27^{+0.04}_{-0.03}$	23.4
			3C 434.1 + G093.7–00.2					
5	[Model 4] + point source	18.1	−1011508.73	9	13.5	322.19 ± 0.04, 50.83 ± 0.04	⋯	⋯
			3C 434.1 + G093.7–00.2 + Outburst					
6	[Model 5] + point source	45.81	−1011485.91	13	51.2	324.997, 52.972	⋯	⋯

Note. The first column designates the model number, and the second column shows the spatial model tested. The third column corresponds to the TS value for each component included in the spatial model. The fourth column provides the LogLikelihood estimate. The fifth column presents the dof introduced by the spatial model. The sixth column quantifies the comparison of the fit quality of each tested spatial model compared to the single point source (4FGL J2123.9+5158). The seventh, eighth, and ninth columns show position, extension (radius and σ for disk and 2D-Gaussian, respectively), and extension significance of the fitted components of the spatial models tested, where applicable. The second row shows the fit quality using all 4FGL-DR4 sources to construct our model, except 4FGL J2123.9+5158, the source currently used in the catalog to describe gamma-ray emission spatially coincident with 3C 434.1. Then we add sources iteratively for 3C 434.1, G093.7–00.2, and the outburst to the model. As demonstrated in the last row, the best-fit model (6) significantly improves the current description of the gamma-ray emission from this region by incorporating gamma-ray emission from the two SNRs and the newly discovered transient.

an additional 2.5 yr of LAT data since the release of the 4FGL-DR4 catalog, we investigate whether sufficient data have been accumulated to detect gamma-ray signatures from G093.7–00.2, which is also considered to interact with dense material (H I structures). The zoomed-in PS map, depicted in the right panel of Figure 2, reveals a gamma-ray enhancement from the central regions of the remnant, albeit much fainter compared to 3C 434.1. Using model 4, found to best characterize 3C 434.1 in the previous section, we introduce an additional component to model the emission coincident with SNR G093.7–00.2 and test for extension. As in Section 3.1, both geometrical templates and the remnant CGPS map were examined. No evidence for extension is found; therefore, the source is modeled as a point source.

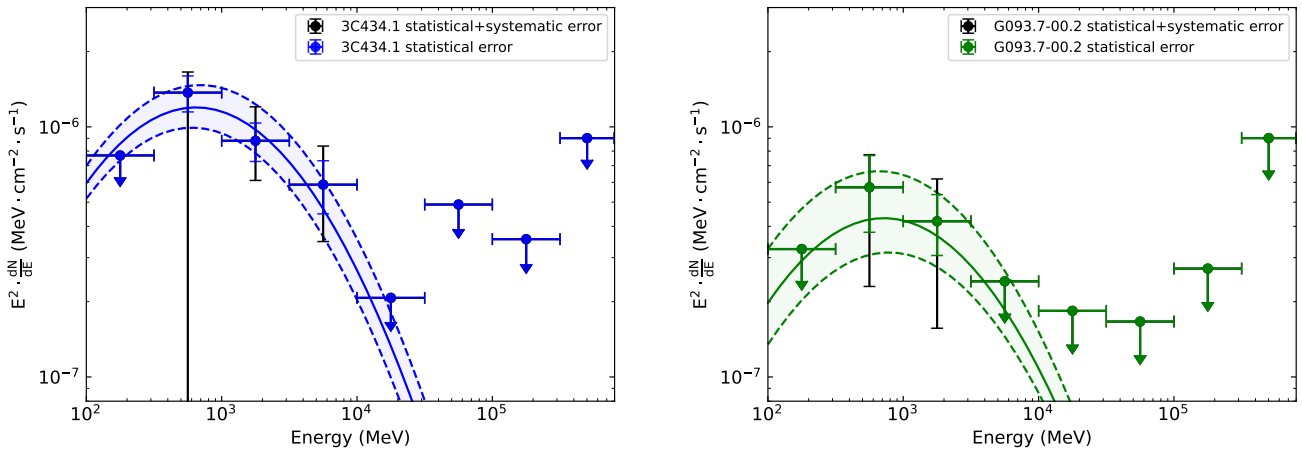

Figure 3. The Fermi-LAT SEDs for 3C 434.1 (left panel) and G093.7–00.2 (right panel) spanning the 100 MeV–800 GeV energy range. Systematic contributions are depicted in black in both panels, corresponding to the energy intervals where a statistically significant gamma-ray signal was detected.

However, this result may be attributed to limited statistics, as a maximum TS $\sim$ 18 was obtained when modeling the gamma-ray emission with a point source. Consequently, we detected a gamma-ray signal from G093.7–00.2 with a significance level of 3.5σ for energies exceeding 1 GeV, for the 4 dof introduced by the point source added in model 5 (see Table 1). Notably, there is evidence of curvature assuming the LogParabola (LP) spectrum when decreasing the lower energy bound of the analysis from 1 GeV to 100 MeV (described more in Section 4), which achieves a TS = 22.9, a 4σ detection significance >1 GeV. The gamma-ray emission appears to be confined within the radio shell of the remnant, and the updated model 5 reported in Table 1 significantly improves the fit quality compared to models 1 and 4.

3.3. Outburst Event and Global Spatial Model

Analyzing 16.5 yr of LAT data, we detected a significant enhancement of the gamma-ray emission with a corresponding TS of 45.81 at energies >1 GeV, best represented by a single point source at the location of the outburst: R.A.: 324°.997, decl.: 52°.972, with an uncertainty of 0°.11—95% confidence, as determined by utilizing the *fermipy* `localization` task. This corresponds to a 6σ detection significance, accounting for the 4 dof a point source introduces, over the 16.5 yr (upper left panel of Figure 1). This is already indicative of the presence of a quiescent signal over a longer period compared to the 3 day outburst event (as described below). We note that an Astronomer's Telegram (ATel) report (C. C. Cheung et al. 2024) has been issued for this event, suggested to be a blazar, as the brightness of the event activated the LAT transient alert systems on August 7, 2024. Upon further inspection, we note that the event had not been cataloged. The source is absent from the 4FGL-DR4 catalog, which utilizes 14 yr of Fermi-LAT data. Additionally, the source is not present in the TS map of the region provided by V. Doroshenko et al. (2019), where weak gamma-ray signals from the two nearby SNRs are reported, as mentioned in Section 1. Consequently, the source may either be a new gamma-ray emitter that became bright in the last 2.5 yr of LAT operation (post-August 2022) or a transient event with an outburst energetic enough to leave a strong signature in the 16.5 yr LAT maps. The latter is further corroborated by producing the Fermi PS maps segmenting the 16.5 yr data sets into smaller time intervals, showing the absence of the source in the first 14 yr of data (upper right panel of Figure 1) and its significant presence in the last 2.5 yr (lower left panel of Figure 1).

Although the gamma-ray outburst is detected over a 3 day period (as deduced from the time-resolved analysis described in Section 5.1), it is sufficiently energetic to leave an imprint on the 16.5 yr Fermi maps at a $\sim$6σ level (see upper left panel of Figure 1). In this regard, its inclusion in the model is necessary to model the nearby sources adequately, especially the two SNRs. Consequently, we incorporate a second point source in our model, which is favored over extended emission templates tested (a radial disk and a radial Gaussian), centered on the coordinates obtained from the *fermipy* `localization` task. The final global model, designated as model 6 in Table 1, incorporates three new sources: a radial disk describing the gamma-ray emission from 3C 434.1 instead of the 4FGL J2123.9+5158 source, a point source describing the gamma-ray emission from G093.7–00.2, and a point source describing the gamma-ray outburst event. The final global model provides a substantially improved fit that adequately describes the gamma-ray emission from this analysis region.

4. Spectral Analysis

The spectral analysis of all three sources was conducted over a broad energy range of 100 MeV–800 GeV. We adopt model 6 from Table 1 as our updated global spatial model for the spectral fitting. Prior to conducting the spectral analysis, a PS map for energies >100 MeV was generated and subsequently examined to determine whether the observed enhancements in gamma-ray emission (three sources of interest) exhibited any morphological deviations attributable to lower energy contributions and/or whether there are nearby soft gamma-ray sources absent in the maps exceeding 1 GeV that, if not modeled, might contaminate the spectra of our sources of interest. No model alterations were deemed necessary.

4.1. SNRs

A power law, a LP, and a power law with a super-exponential cutoff (PLSC) were tested as spectral models for the two SNRs. Both SNRs exhibit a photon energy distribution best characterized by a LP showing significant spectral curvature at around $\sim$1 GeV, which is indicative of hadronically induced gamma-ray emission (refer to Section 6 for further discussion), as displayed in Figure 3, with the best-fit parameters provided in Table 2. The spectral energy distribution (SED) plots were obtained by dividing the

Table 2
SNR Spectral Parameters >100 MeV

Object	Spectral Model	Index (α, β)	Energy Flux (MeV cm^{-2} s^{-1})	TS_{LP}	TS_{PLSC}
3C 434.1	LP	$1.25 \pm 0.12 \pm 0.30$, $0.20 \pm 0.02 \pm 0.02$	$4.17 \pm 0.54 \pm 1.12 \times 10^{-6}$	20.4	17.9
G093.7–00.2	LP	$1.21 \pm 0.20 \pm 0.25$, $0.19 \pm 0.02 \pm 0.03$	$1.54 \pm 0.40 \pm 0.63 \times 10^{-6}$	10.8	9.8

Note. Both the spectral slope (α) and curvature (β), as defined in P. L. Nolan et al. (2012) for the LP, are listed. The first error represents statistical uncertainties, whereas the second error accounts for both statistical and systematic uncertainties (including systematics for upper limits).

Table 3
Transient Spectral Parameters with Statistical Errors >100 MeV

Data Sets	Spectral Model	Index	Energy Flux (MeV cm^{-2} s^{-1})	TS	TS_{LP}	TS_{PLSC}
6 hr (Aug 7, 12:00 to Aug 7, 18:00—2024)	Power law	1.73 ± 0.16	$2.36 \pm 1.58 \times 10^{-3}$	49.6	5.1	5.6
18 hr (Aug 7, 12:00 to Aug 8, 06:00—2024)	Power law	1.77 ± 0.11	$1.40 \pm 0.60 \times 10^{-3}$	106.8	5.7	6.2
3 days (Aug 6, 12:00 to Aug 9, 12:00—2024)	Power law	1.96 ± 0.04	$4.77 \pm 0.54 \times 10^{-4}$	157.8	2.9	4.6
16.5 yr (Aug 8, 2008, to Feb 13, 2025)	Power law	2.45 ± 0.09	$3.19 \pm 0.49 \times 10^{-6}$	59.1	1.1	1.7

examined energy range into eight logarithmic energy bins. The first seven are of equal width. The final bin is narrower, covering the ~320–800 GeV energy range. Photon flux computation was performed in each time interval. Energy intervals with TS < 4 are presented as 95% upper limits. This finding aligns with expectations, given the strong evidence supporting a hadronic interpretation of the gamma-ray data due to the SNRs' association with dense material. Finally, we investigated the impact of systematic uncertainties arising from the Galactic diffuse background, the effective area, and the selected spatial template on our spectral analysis results. To address the first two sources of systematic uncertainty, we applied the approach introduced in F. Acero et al. (2016). For the modeling of 3C 434.1, we utilized the alternative spatial template constructed from its radio shape, which is the second-best-fit spatial template for 3C 434.1—Model 2 in Table 1, to evaluate the impact of systematic uncertainty introduced by the chosen spatial template. The results, added in quadrature, are depicted in black, showing total systematics on the corresponding SEDs.

4.2. Outburst

The outburst spectral analysis was performed focusing both on the outburst event ($\leqslant$3 days, as determined by the time-resolved analysis performed in Section 5.1) and using all available data sets (16.5 yr) from the location of the potential gamma-ray source producing the outburst. As in Section 4.1, the same conventions applied to the SED plot construction (i.e., energy bin widths and TS thresholds for upper limits). A power law, a LP, and a PLSC model were tested as spectral models for the point source reproducing the gamma-ray emission from the outburst position. As the fit improvements introduced by the latter two models were insignificant and the curvature significance is only marginally above the 2σ level for the short-term time intervals or $<2\sigma$ for the 16.5 yr time interval, a simple power law was adopted for all four chosen time intervals, as presented in Table 3. Notably, a significant alteration in the spectral shape of the outburst was observed when comparing data sets from all 3 days with those from 18 and 6 hr of the event peak. The change of the spectral shape during the outburst can be an indication of an acceleration mechanism at work in the gamma-ray source at that time. Nonetheless, all three short-term time intervals exhibit a hard spectrum $\Gamma < 2$ (see Table 3). Figure 4 (upper left panel) presents the gamma-ray SEDs of the three short-term time intervals, and the corresponding best-fit spectral results are reported in Table 3. In contrast to the short-term time intervals, the 16.5 yr time interval is characterized by a soft spectral index of 2.45 ± 0.09, as illustrated in the upper right panel of Figure 4 and the bottom row of Table 3.

5. Outburst Inspection

5.1. Time-resolved Analysis of the Outburst

To further elucidate the characteristics of the source associated with the outburst event, we initially constructed the source light curve in both the 100 MeV to 1 GeV and the 1 GeV to 800 GeV energy bands over 16.5 yr of data, segmented into half-year intervals. The light curves reveal that this is a transient source, detected primarily at >1 GeV, with no significant outburst recorded by Fermi-LAT prior to August 7, 2024. This is also evidenced in Figure 1. Consequently, we proceeded to construct a light curve with single-month time bins, which, although showed no outburst event prior to August 7, 2024, evidently indicated the presence of some quiescent signal (a gamma-ray signal with TS ~ 30 was obtained in a few bins that is washed out when analyzing long time intervals) with no clear periodicity, followed by more precise temporal localization using single-day and 6 hr bins. This analysis determined that the transient event spanned 3 days, from August 6 to August 9, 2024, with the outburst peaking on August 7, 2024, specifically from August 7 at noon to August 7 at 6 pm, that is 744724805 to 744746405 MET, as indicated by the gray shaded regions in the lower left panel of Figure 4. A significant detection of 4σ, 10σ, and 5σ at >1 GeV was obtained throughout the 3 day outburst period. The corresponding light curve at >1 GeV is presented with both single-day and 6 hr time bins centered on the event peak (lower left panel of Figure 4). The data with error bars correspond to TS = 17.8, 47.2, 29.6, 31.9, 15.7 for 6 hr bins and TS = 18.7, 105, 24 for the single-day bins. A 3σ threshold has been used

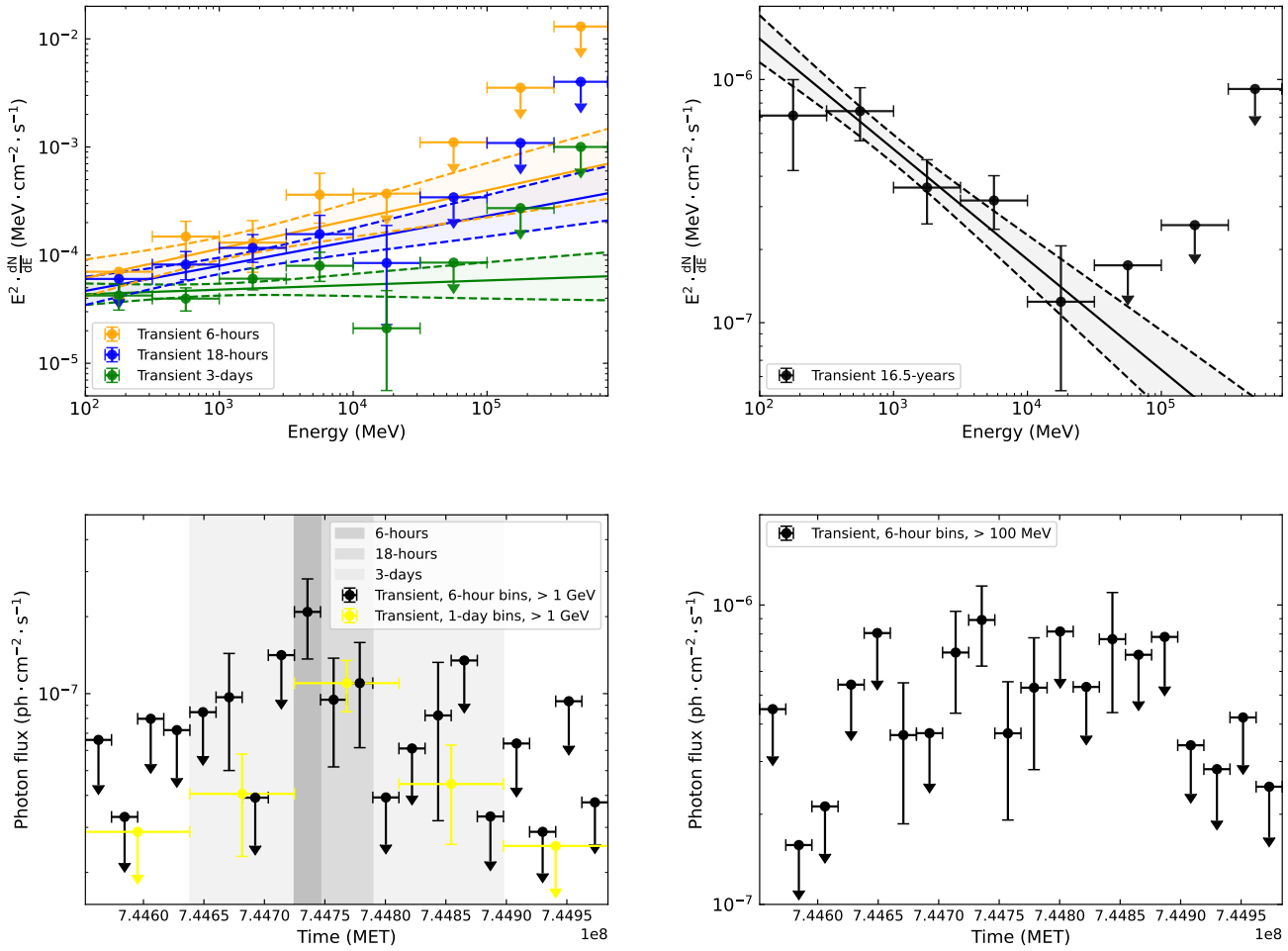

Figure 4. Outburst SEDs and light curves. The top panels present the LAT SEDs in the 100 MeV to 800 GeV energy range. Upper left panel: LAT SEDs using 3 days from August 6, 12:00 to August 9, 12:00 (MET: 744638405 to 744897605), 18 hr from August 7, 12:00 to August 8, 06:00 (MET: 744724805 to 744789605), and 6 hr from August 7, 12:00 to August 7, 18:00 (MET: 744724805 to 744746405) of data sets in green, blue, and orange, respectively. Upper right panel: LAT SED from the location of the outburst using 16.5 yr of data from August 8, 2008, to February 13, 2025 (MET: 239557417 to 761167438). The bottom panels depict the LAT light curves for the 5 days period from August 5, 12:00 to August 10, 12:00 (MET: 744552005 to 744984005) centered at the event peak, >1 GeV (left) and >100 MeV (right), with single-day bins in yellow and 6 hr bins in black.

to set upper limits. For the sake of completeness, the outburst light curve >100 MeV is also provided (lower right panel of Figure 4).

5.2. Possible Multiwavelength Counterparts to the Outburst

No infrared, optical, or X-ray follow-up observations were conducted from the transient position during the outburst event. To gain further insight into the nature of the detected gamma-ray outburst, potential associations with persistent multiwavelength counterparts were explored. No definitive X-ray counterpart has been identified that would facilitate a distance measurement of the source. Nevertheless, the transient position was observed serendipitously by the Swift X-Ray Telescope (XRT; D. N. Burrows et al. 2005) in pointings obtained in Target IDs 3102311 (March to April 2021) and 3103379 (January to March 2022) with 4.8 ks cumulative exposure at the position of TXS 2138+527 (the most likely source for the outburst, as explained below). Using the Swift-XRT point-source pipeline[10] (P. A. Evans et al. 2020), a low-significance (signal-to-noise ratio = 2.3) point source with 11 observed counts in the 0.3–10 keV range was found at a position, R.A., decl. (J2000) = $324.^{\circ}9708$, $53.^{\circ}0054$ (error radius, $r = 7.''8$, 90% confidence) that is offset by $6.''4$ from the radio position. The background subtracted rate of $3.0^{+1.1}_{-0.9}$ ks^{-1} translates to an observed 0.3–10 keV flux of $3.8^{+2.8}_{-2.3} \times 10^{-13}$ erg cm^{-2} s^{-1} for a single power-law fit (photon index = $1.2^{+2.6}_{-1.3}$) to the spectrum.

Notably, the gamma-ray outburst is offset by $0.^{\circ}04$ from the unidentified flat-spectrum ($\alpha = -0.46$) radio source TXS 2138 +527 (also known as NVSS J213953+530016), initially reported in S. Zoonematkermani et al. (1990). The latter source is compact on milliarcsecond scales (K. Immer et al. 2011), a common characteristic of blazars. In addition, the outburst is separated by $0.^{\circ}08$ from the hydrogen-rich white dwarf Gaia DR3 2173377013704183936 (DA spectral type). Thus, considering its duration, as evidenced by the obtained light curves, the most probable origin of the gamma-ray event is either a nova event supported by the spatially coincident white dwarf (WD) or a blazar flare supported by the spatial coincidence with NVSS J213953+530016. In the latter scenario, it is observed that the radio compact source is documented in L. Y. Petrov & Y. Y. Kovalev (2025), albeit without redshift information. In the former scenario, it is important to note that a nova event would necessitate the

[10] https://www.swift.ac.uk/user_objects/

involvement of a WD in a binary system. The recently discovered WD within the gamma-ray outburst's uncertainty position has not yet been reported as part of a binary system (refer to P. Dufour et al. 2017; O. Vincent et al. 2024). In the absence of a main-sequence companion, its classification as a possible nova candidate is precluded. However, this newly discovered WD has not been thoroughly studied. Alternatively, an undetected WD in a binary system could be located along the line of sight in the direction of the gamma-ray outburst.

The spectral hardness of the gamma-ray outburst, as evidenced by the LAT SEDs of the three short-term chosen time intervals on the upper left panel of Figure 4 and by the corresponding spectral indices reported in Table 3, is atypical for novae events but rather common among blazars in flare (e.g., G. Ghisellini et al. 2013). The 6σ detection of the source over a span of 16.5 yr indicates a quiescent signal over a longer period (or highly periodic) with a softer spectrum. This is further corroborated by both the gamma-ray SED obtained over the same period, which shows a soft spectrum of $\Gamma \sim 2.4$ in contrast to the hard indices obtained for the three short-term time intervals during the outburst (refer to Table 3 for a direct comparison of the spectral indices), and by the single-month time bin analysis that showed the presence of some quiescence signal, though without a clear periodicity. Although not analyzed in this study, we examined the Fermi All-Sky Variability Analysis (FAVA) tool (M. Ackermann et al. 2013; S. Abdollahi et al. 2017), as an additional six months of LAT data have been collected since the initiation of this project. We observed renewed activity at and above the $>5\sigma$ level from the transient position one year following the outburst, specifically from July 14, 2025, to July 21, 2025 (MET: 774200618 to 774805418), and from July 21, 2025, to July 28, 2025 (MET: 774805418 to 775410218), respectively. These findings further contradict the nova interpretation. To this end, the flat radio spectrum of NVSS J213953+530016, in conjunction with the derived gamma-ray SED for the full data sets, suggests an FSRQ nature for the source, the power-law index of $\sim$2.4 being characteristic of this blazar class (M. Ajello et al. 2020). Although an FSRQ nature for the source is clearly favored, it is important to note that a BL Lac object cannot be excluded solely based on the gamma-ray spectral shape (refer to A. A. Abdo et al. 2010a for photon index comparisons between blazar classes). Nevertheless, additional multiwavelength observations targeting the source and its future monitoring are strongly recommended to conclusively determine its origin.

6. Discussion and Conclusions

In this study, we present an analysis of the gamma-ray emission found to be spatially coincident with two Galactic SNRs, namely, 3C 434.1 and G093.7–00.2. Both SNRs were reported as undetected in the first Fermi-LAT SNR catalog. The study by V. Doroshenko et al. (2019), which primarily focuses on the X-ray emission of 3C 434.1, indicates weak gamma-ray signals at the 3.2σ and 1.7σ levels for 3C 434.1 and G093.7–00.2, respectively, without providing a gamma-ray morphological or spectral analysis. Given that both SNRs are believed to interact with dense material, they are strong candidates for hadronically induced gamma-ray emission. Utilizing 16.5 yr of LAT data, we detect enhanced gamma-ray emission with significances of 7.2σ and 4.5σ, spatially coincident with 3C 434.1 and G093.7–00.2, respectively. Consequently, we add two new objects to the pool of gamma-ray emitting SNRs. We conducted a comprehensive morphological and spectral analysis of the gamma-ray emission for both remnants. A significant extension for the gamma-ray source spatially coincident with the 3C 434.1 SNR was obtained ($TS_{ext} = 23.4$), in excellent spatial agreement with the remnant's radio shell. Notably, the gamma-ray emission seems to be enhanced in the remnant's western hemisphere, whereas the radio and X-ray bands exhibit significant emission enhancement in the eastern hemisphere. However, it is the eastern hemisphere that is most likely interacting with the molecular cloud at 3 kpc, as reported in I.-G. Jeong et al. (2013). This study thus provides strong evidence that the SNR generates the observed gamma-ray emission as it interacts with the molecular cloud located at 3 kpc. Subsequently, this interaction offers a reliable distance estimate for the remnant itself.

The gamma-ray emission from G093.7–00.2 does not display significant extension and is well confined within the SNR shell. We note that limited data statistics might hinder a firm detection of the source extension. While we cannot exclude the possibility that the gamma-ray emission originates from an associated PWN, it is noteworthy that neither PWNe identified in other wavelengths nor pulsars have been detected in this region of the sky. The blind pulsation search performed with the `gtpspec` fermitools task, aiming at exploring a potential pulsar association, did not yield conclusive results due to the faint nature of the source and is therefore not presented in this work. It is important to note that the absence of gamma-ray pulsations does not definitively indicate the absence of a pulsar. While gamma-ray pulsations may serve as key indicators, there are significant hindrances, apart from a weak signal, that might impede such detection (see, e.g., P. M. Saz Parkinson & Fermi LAT Collaboration 2013 and references therein for a discussion). Nonetheless, the absence of an extension in the LAT data from an $80'$ SNR (as observed in radio) may suggest that the gamma-ray source is not associated with the remnant. Alternatively, it is conceivable that the remnant interacts locally with dense material, which could be responsible for the point-like gamma-ray emission. We aim to revisit the SNR with additional years of LAT data sets to either confirm or challenge the association of the remnant with this gamma-ray source. Currently, there are no other known astrophysical objects in this region that could account for the observed gamma-ray emission. As such, G093.7–00.2 is a prime candidate to explain the observed gamma-ray excess.

The soft gamma-ray SEDs of both SNRs, exhibiting an apparent spectral curvature at $\sim$1 GeV, are consistent with the proton–proton interaction scenario rather than the inverse Compton emission scenario from accelerated electrons, further supporting the hadronic nature of the gamma-ray counterparts of the two remnants and their interaction with dense material. We note that such a hadronic origin applies to G093.7–00.2 only if the gamma-ray emission is confirmed to be of SNR nature. We emphasize that the only definitive hadronic signature is the pion decay bump and that spectral curvature alone cannot provide direct information about emission mechanisms. It is not that a LP determines the origin of gamma-rays; rather, it is typically the energy interval at which the curvature appears. When comparing young, typically

leptonic gamma-ray emitting SNRs with middle-aged hadronic SNRs, there is a common trend for gamma-ray emission to peak and exhibit spectral curvature at teraelectronvolt and gigaelectronvolt energies, respectively (see, e.g., X. Guo & X. Liu 2024). Thus, a spectral curvature at gigaelectronvolt energies (typically around 1 GeV) favors a hadronically dominated gamma-ray emission component. A multiwavelength SED modeling may provide more insight into the emission mechanism, but the detection of a hard X-ray filament for 3C 434.1 (V. Doroshenko et al. 2019), possibly originating from the interaction of the shock with the dense surrounding medium, supports a hadronic interpretation of the observed gamma-ray emission (see, e.g., E. G. Berezhko & H. J. Völk 2008). Consequently, and in the absence of significant nonthermal X-ray signatures from either remnant—except for a single likely nonthermal hard filament reported in V. Doroshenko et al. (2019), which spans only a small southern region (5′) of 3C 434.1, which is hardly discernible from the dominant thermal X-ray component and does not spatially coincide with the western enhanced SNR gamma-ray hemisphere—we encourage future work involving more robust multiwavelength data, particularly in X-rays, to allow for robust nonthermal modeling constraints and consequently provide further insight into the emission mechanisms and properties of the SNRs.

In close proximity to the two SNRs, a gamma-ray outburst was observed in late 2024. The discovery of the gamma-ray outburst source was reported in an ATel report issued by C. C. Cheung et al. (2024). We present a detailed analysis of it here. The transient event, lasting 3 days, was identified using Fermi-LAT, with its peak occurring on August 7, 2024. Within the positional uncertainty of approximately $0.^{\circ}11$ (95% confidence), the flat-spectrum radio source TXS 2138+527 (or NVSS J213953+530016) emerged as the most plausible candidate associated with the outburst, situated at $0.^{\circ}04$ from the event's best-fit position. An FSRQ origin of the detected transient gamma-ray source appears more probable. In the scenario that the gamma-ray emission originates from a FSRQ and considering the hard gamma-ray spectrum obtained for the short 6 hr, 18 hr, and 3 days time intervals from the event peak (consistent with the harder-when-brighter trend observed in FSRQs; A. A. Abdo et al. 2010b; J. Deng & Y. Jiang 2025), the gamma-ray emission is most likely the result of inverse Compton scattering on an external photon field, termed as external Compton (EC), from the AGN accretion disk and/or the broad line region and/or the dusty torus (C. D. Dermer & R. Schlickeiser 1993; M. Boettcher et al. 1997; M. Błażejowski et al. 2000; M. Hayashida et al. 2012; M. Böttcher et al. 2013), thereby indicating a leptonic origin. Future observations in the optical, X-ray, and infrared can determine the more likely origin.

The present study elucidates the importance of continuous monitoring of the whole sky in gamma rays to detect exotic transient events, the uniqueness of such outburst detections for which follow-up studies should be prioritized aiming at determining their source class, as well as how gamma-ray data can enhance our understanding of the acceleration mechanisms and particle populations in distinct SNRs, and provide critical information regarding intrinsic properties such as their distance.

Acknowledgments

The Fermi LAT Collaboration acknowledges generous ongoing support from a number of agencies and institutes that have supported both the development and the operation of the LAT as well as scientific data analysis. These include the National Aeronautics and Space Administration and the Department of Energy in the United States, the Commissariat à l'Energie Atomique and the Centre National de la Recherche Scientifique/Institut National de Physique Nucléaire et de Physique des Particules in France, the Agenzia Spaziale Italiana and the Istituto Nazionale di Fisica Nucleare in Italy, the Ministry of Education, Culture, Sports, Science and Technology (MEXT), High Energy Accelerator Research Organization (KEK) and Japan Aerospace Exploration Agency (JAXA) in Japan, and the K. A. Wallenberg Foundation, the Swedish Research Council and the Swedish National Space Board in Sweden. Additional support for science analysis during the operations phase is gratefully acknowledged from the Istituto Nazionale di Astrofisica in Italy and the Centre National d'Etudes Spatiales in France. This work performed in part under DOE Contract DE-AC02-76SF00515.

Facility: Fermi-LAT.

Software: fermipy (M. Wood et al. 2017).

Author Contributions

M.M. conducted the Fermi-LAT data analysis, which resulted in the identification of the gamma-ray counterpart of 3C 434.1, provided substantial evidence for gamma-ray emission from G093.7–00.2, and conclusively determined the origin of the late-2024 gamma-ray outburst. M.M. was also responsible for the manuscript preparation. All coauthors participated in interpreting the results and providing critical feedback that shaped the final version of the manuscript.

ORCID iDs

Miltiadis Michailidis https://orcid.org/0009-0008-3653-1109
Marianne Lemoine-Goumard https://orcid.org/0000-0002-4462-3686
Niccolo Di Lalla https://orcid.org/0000-0002-7574-1298
Nicola Omodei https://orcid.org/0000-0002-5448-7577
C. C. Cheung https://orcid.org/0000-0002-4377-0174

References

Abdo, A. A., Ackermann, M., Ajello, M., et al. 2010a, ApJ, 715, 429
Abdo, A. A., Ackermann, M., Ajello, M., et al. 2010b, ApJ, 710, 1271
Abdollahi, S., Acero, F., Baldini, L., et al. 2022, ApJS, 260, 53
Abdollahi, S., Ackermann, M., Ajello, M., et al. 2017, ApJ, 846, 34
Acero, F., Ackermann, M., Ajello, M., et al. 2016, ApJS, 224, 8
Ackermann, M., Ajello, M., Albert, A., et al. 2013, ApJ, 771, 57
Ajello, M., Angioni, R., Axelsson, M., et al. 2020, ApJ, 892, 105
Akaike, H. 1974, ITAC, 19, 716
Baldini, L., Ballet, J., Bastieri, D., et al. 2021, ApJS, 256, 13
Ballet, J., Bruel, P., Burnett, T. H., Lott, B. & The Fermi-LAT collaboration 2023, arXiv:2307.12546
Berezhko, E. G., & Völk, H. J. 2008, A&A, 492, 695
Blandford, R. D., & Rees, M. J. 1978, PhyS, 17, 265
Błażejowski, M., Sikora, M., Moderski, R., & Madejski, G. M. 2000, ApJ, 545, 107
Boettcher, M., Mause, H., & Schlickeiser, R. 1997, A&A, 324, 395
Böttcher, M., Reimer, A., Sweeney, K., & Prakash, A. 2013, ApJ, 768, 54
Bruel, P. 2021, A&A, 656, A81
Bruel, P., Burnett, T. H., Digel, S. W., et al. 2018, arXiv:1810.11394
Burrows, D. N., Hill, J. E., Nousek, J. A., et al. 2005, SSRv, 120, 165

Caswell, J. L. 1970, A&A, 7, 59
Chaty, S. 2012, in Twelfth Marcel Grossmann Meeting on General Relativity, ed. A. H. Chamseddine (Singapore: World Scientific), 1001, doi:10.1142/9789814374552_0116
Cheung, C. C., Marti-Devesa, G., & Bernard, D. 2024, ATel, 16760, 1
Chevalier, R. A., & Liang, E. P. 1989, ApJ, 344, 332
Deng, J., & Jiang, Y. 2025, ApJ, 983, 128
Dermer, C. D., & Schlickeiser, R. 1993, ApJ, 416, 458
Doroshenko, V., Malyshev, D., Pühlhofer, G., et al. 2019, A&A, 631, A179
Dufour, P., Blouin, S., Coutu, S., et al. 2017, in ASP Conf. Ser. 509, 20th European White Dwarf Workshop, ed. P. E. Tremblay, B. Gaensicke, & T. Marsh (San Francisco, CA: ASP), 3
Evans, P. A., Page, K. L., Osborne, J. P., et al. 2020, ApJS, 247, 54
Foster, T. 2005, A&A, 441, 1043
Foster, T., & Routledge, D. 2003, ApJ, 598, 1005
Gao, X. Y., Han, J. L., Reich, W., et al. 2011, A&A, 529, A159
Ghisellini, G., Tavecchio, F., Foschini, L., Bonnoli, G., & Tagliaferri, G. 2013, MNRAS, 432, L66
Giuliani, A., & Cardillo, M. 2024, Univ, 10, 203
Green, D. A. 2025a, JApA, 46, 14
Green, D. A. 2025b, yCat: VII/297. Originally published in: 2025JApA...46...14G
Guo, X., & Liu, X. 2024, ApJ, 975, 272
Hayashida, M., Madejski, G. M., Nalewajko, K., et al. 2012, ApJ, 754, 114
Immer, K., Brunthaler, A., Reid, M. J., et al. 2011, ApJS, 194, 25
Jeong, I.-G., Koo, B.-C., Cho, W.-K., et al. 2013, ApJ, 770, 105
Landecker, T. L., Higgs, L. A., & Roger, R. S. 1985, AJ, 90, 1082
Mantovani, F., Nanni, M., Salter, C. J., & Tomasi, P. 1982, A&A, 105, 176
Nolan, P. L., Abdo, A. A., Ackermann, M., et al. 2012, ApJS, 199, 31
Petrov, L. Y., & Kovalev, Y. Y. 2025, ApJS, 276, 38
Rohlfs, K. 1990, Tools of Radio Astronomy (Berlin & Heidelberg: Springer-Verlag)
Saz Parkinson, P. M. & Fermi LAT Collaboration 2013, in IAU Symp. 291, Neutron Stars and Pulsars: Challenges and Opportunities after 80 years, ed. J. van Leeuwen (Cambridge: Cambridge Univ. Press), 81, doi:10.1017/S174392131202323X
Sun, X. H., Reich, P., Reich, W., et al. 2011, A&A, 536, A83
Urry, C. M., & Padovani, P. 1995, PASP, 107, 803
Uyaniker, B., Kothes, R., & Brunt, C. M. 2002, ApJ, 565, 1022
Vincent, O., Barstow, M. A., Jordan, S., et al. 2024, A&A, 682, A5
Wang, S., Zhang, C., Jiang, B., et al. 2020, A&A, 639, A72
Willis, A. G. 1973, A&A, 26, 237
Wood, M., Caputo, R., Charles, E., et al. 2017, ICRC (Busan), 301, 824
Yamamoto, F., Hasegawa, T., Sawada, T., et al. 2002, in 8th Asian-Pacific Regional Meeting, Volume II, ed. S. Ikeuchi, J. Hearnshaw, & T. Hanawa (Tokyo: Astronomical Society of Japan), 235
Yang, K. S., & Dickel, J. R. 1965, AJ, 70, 300
Zhao, H., Jiang, B., Li, J., et al. 2020, ApJ, 891, 137
Zoonematkermani, S., Helfand, D. J., Becker, R. H., White, R. L., & Perley, R. A. 1990, ApJS, 74, 181